JOURNAL OF THERMOPHYSICS AND HEAT TRANSFER
Vol. 10, No. 3, July–September 1996

Technical Notes

TECHNICAL NOTES are short manuscripts describing new developments or important results of a preliminary nature. These Notes cannot exceed 6 manuscript pages and 3 figures; a page of text may be substituted for a figure and vice versa. After informal review by the editors, they may be published within a few months of the date of receipt. Style requirements are the same as for regular contributions (see inside back cover).

Comparison of Mass Sensitivities of 10- and 15-MHz Quartz Crystal Microbalances

A. P. M. Glassford*
Lockheed Martin Corporation, Sunnyvale, California 94089
and
D. A. Wallace†
QCM Research, Laguna Beach, California 92652

Introduction

QUARTZ crystal microbalances (QCM) are widely used in the aerospace community for measuring surface deposit mass in many contamination-related applications, such as materials characterization tests,[1,2] molecular contaminant deposition kinetics,[3] and contamination monitoring during ground testing,[4] and on orbiting spacecraft.[5] Typically, 10- and 15-MHz QCMs are used for these applications. If apparently anomalous test results are obtained when both types of QCM are used side-by-side in the same application, their relative mass sensitivity is sometimes questioned. This Note describes an experimental determination of the ratio of the mass sensitivities of 10- and 15-MHz QCMs, whose objective was to put this issue to rest.

Mass deposits encountered in contamination characterization are small enough for the assumption of constant deposit velocity and zero losses to be valid, and so the theoretical mass sensitivity of a QCM, S Hz cm^2/g, is given by Eq. (1) (Ref. 6),

$$S = 2f_c^2/\rho_q v_q \tag{1}$$

where f_c is the sensing crystal frequency, Hz; ρ_q is the density of quartz, 2.650 g/cm^3; and v_q is the shear wave velocity in quartz, 3340 m/s. For a 10-MHz QCM, the theoretical mass sensitivity of 0.226×10^9 Hz cm^2/g has been confirmed by comparison with a vacuum microbalance to within ±1% (Refs. 7 and 8), whereas similar calibrations of QCMs with various other frequencies have shown agreement with theory to better than ±2% (Ref. 6). The mass sensitivity of a 10-MHz QCM has been verified at low temperature in vacuum by comparing the measured evaporation rate of water deposits from the QCM sensing crystal to the evaporation rates predicted using published vapor pressure data for water and the langmuir equation.[9] Given the proven validity of Eq. (1), the ratio of the mass sensitivities of the 15- and 10-MHz QCMs, S_{15}/S_{10}, should be equal to the square of the sensing crystal frequency ratio, or 2.25.

The mass sensitivity comparison was made by measuring the frequency changes of 10- and 15-MHz QCMs while both were held at 85 K in vacuum and exposed to the same flux of water vapor. The condensation coefficient for water on ice should be identical for the two QCMs and should be close to unity.[10] The evaporation rate of ice at 85 K is less than 10^{-22} g/cm^{2}s (Ref. 11), and therefore negligible. Once ice has completely covered both crystals, the net deposition rates on the QCMs should be identical, and S_{15}/S_{10} should equal the ratio of the measured frequency changes.

QCM Description

The QCMs compared were the 10-MHz MK 9 and two nominally identical 15-MHz MK 18 QCMs made by QCM Research. Both models use a sensing crystal, a matched reference crystal to offset temperature effects on frequency, and a temperature-sensing element positioned as close as possible to the crystals. The output is the beat frequency of the sensing and reference crystals. The MK 9 crystal assembly uses 1.247 ± 0.025-cm-diam plano–plano crystals oscillated at their fundamental frequency, and a DIN 43760 standard platinum resistance thermometer (PRT). The crystals are optically polished and have full surface vapor-deposited gold electrodes. The active area on each crystal is 0.317 cm^2. The MK 18 crystal assembly uses similar crystals, and a silicon diode temperature sensing element. The MK 9 has been described elsewhere.[9] The MK 18 is physically similar to the MK 9, but has a shorter case.

Apparatus

The apparatus is shown in Fig. 1. The QCMs are mounted to the underside of a liquid nitrogen reservoir by struts that are sized and positioned such that geometrically similar QCMs have the same view factor to the effusion cell orifice. The MK 9 and MK 18 QCMs have slightly different case dimensions and different cell orifice view factors. Their relative view factor ratio was determined by calculation using QCM and ap-

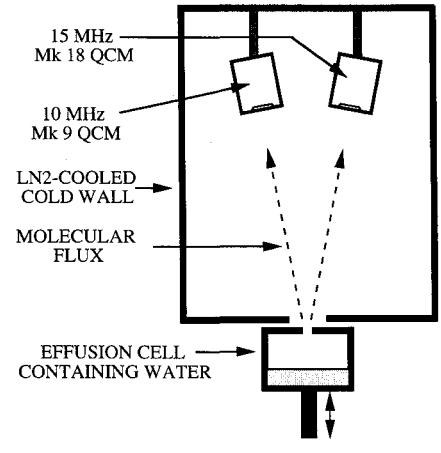

Fig. 1 Schematic of apparatus.

Received Oct. 4, 1995; revision received Jan. 3, 1996; accepted for publication Jan. 4, 1996.

*Senior Staff Engineer, Materials and Processes Control Laboratories, 1111 Lockheed Way. Member AIAA.
†President. Member AIAA.

paratus dimensions after mounting the QCMs. The view factor of the MK 9 crystal was found to be 1.053 times greater than that of the MK 18 crystal.

The source of molecular flux is an effusion cell containing distilled and degassed water. The cell is heated electrically, and is normally cooled by radiative heat loss to the cold walls. It can also be cooled rapidly by pressing it against the cold wall using its mounting rod, which can be moved from outside the vacuum chamber. Since the apparatus did not have a shutter, rapid cooling of the cell was used to interrupt the flux impinging on the QCMs at the end of a test. The time required to reduce the impinging flux to a negligible value was a few minutes. When the cell temperature had fallen below 100 K, the accumulation rate on the 10-MHz QCM at 85 K was less than the resolution limit of about 1 Hz/week or 5×10^{-9} g/cm^2 per week.

Deposition Tests

A deposition test was started by inserting the effusion cell into the test chamber and cooling it to suppress water evaporation by pressing it against the cold wall. The deposition test consisted of heating the cell to a temperature high enough to create an appropriate impingement rate on the QCM surfaces, and measuring the frequencies of the two QCMs, $f_{10}(t_i)$ and $f_{15}(t_i)$, respectively, as functions of time t_i. Deposition was continued until the deposit mass was greater than approximately 10^{-4} g/cm^2, and clearly in the bulk regime. The test was terminated by reducing the impinging flux to a negligible value by pressing the cell against the cold wall. Deposition tests were performed on each of the 15-MHz QCMs in succession. The two data sets are referred to here as 15-A and 15-B. The test procedures were qualitatively similar, except that for 15-A the maximum effusion cell temperature was 220 K and the maximum deposition rate was 3.3×10^{-8} g/cm^{2}s, whereas for 15-B these values were 235 K and 8.8×10^{-8} g/cm^{2}s, respectively.

Results

Assuming all impinging water vapor condenses, the mass deposited on the 10-MHz QCM is equal to the mass deposited on the 15-MHz QCM, multiplied by the view factor ratio of 1.053, Eq. (2),

$$[f_{10}(t_j) - f_{10}(t_i)]/S_{10} = 1.053[f_{15}(t_j) - f_{15}(t_i)]/S_{15} \quad (2)$$

or

$$S_{15}/S_{10} = 1.053[f_{15}(t_j) - f_{15}(t_i)]/[f_{10}(t_j) - f_{10}(t_i)] \quad (3)$$

Using Eq. (3) and the overall frequency change measured from the beginning of deposition on clean QCM surfaces to the end of deposition, S_{15}/S_{10} is calculated to be 2.233 and 2.255 for tests 15-A and 15-B, respectively. Since these numbers are based on the largest frequency changes measured, they might be expected to be the most reliable values for S_{15}/S_{10}. However, the initial stages of deposition on a clean surface involve adsorption, nucleation, and island formation, all of which have surface-dependent kinetics, and the assumption of unity condensation coefficient is valid only after the islands bridge over to form a continuous film of bulk material. For this reason, the S_{15}/S_{10} values based on the overall frequency changes are not reliable.

QCM calibrations[6] are invariably based on relatively thick deposits, to ensure that the deposit is a continuous film of bulk material, the effect of the crystal surface type is eliminated, and the assumption of unity condensation coefficient is valid. For the present tests, the deposit mass at which a continuous film of bulk material was obtained was estimated by calculating S_{15}/S_{10} as a function of deposit mass using Eq. (3) and the frequency changes measured at successive times t_i and t_{i+1}. The mass deposited on the QCMs was assumed to be equal to that on the 10-MHz QCM at time $(t_i + t_{i+1})/2$, and was calculated using Eq. (4),

$$m_d[(t_i + t_{i+1})/2] = \{f_{10}[(t_i + t_{i+1})/2] - f_{10}(t_0)\}/0.226 \times 10^9 \quad (4)$$

where t_0 is the time at the start of deposition. Figure 2 shows S_{15}/S_{10} vs deposit mass. There is considerable variation in S_{15}/S_{10} for smaller deposit mass, but S_{15}/S_{10} becomes relatively constant for larger deposits. The variability at small deposit mass is because of differences in the adsorption/nucleation characteristics of the 10- and 15-MHz crystals. The figure suggests that a continuous film was not obtained until the deposit mass had exceeded about 4×10^{-5} g/cm^2 in the test 15-A, and 2×10^{-5} g/cm^2 in test 15-B. Bridging-over occurred at a lower deposit mass for 15-B than for 15-A because a higher deposition rate was used. The most reliable values for S_{15}/S_{10} are calculated using the frequency changes from the time at which a continuous film was obtained to the end of deposition. These values are 2.230 and 2.245 for tests 15-A and 15-B, respectively.

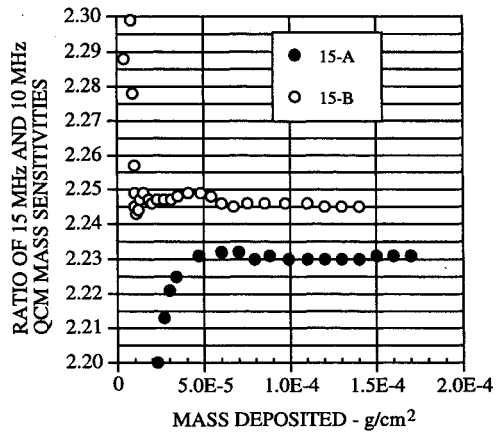

Fig. 2 Ratio of the mass sensitivities of the 15- and 10-MHz QCMs as a function of mass deposited.

Discussion

The frequencies of the measuring crystals are known from supplier data to be within 10 KHz of the nominal 15- and 10-MHz values, and so the theoretical value of S_{15}/S_{10} is 2.250 ± 0.05% or better. The measured S_{15}/S_{10} of 2.230 for 15-A and 2.245 for 15-B agree with the theoretical value to better than 0.9 and 0.2%, respectively. Since the two 15-MHz QCMs were nominally identical, the 0.7% difference between S_{15}/S_{10} for 15-A and 15-B must be because of an experimental reproducibility limitation.

Possible sources of error include frequency, temperature, the assumption of the same condensation coefficient for both QCMs, and view factor measurements. Errors from the first three of these sources are considered negligible. Frequency was measured using the same high-accuracy counter for both QCMs. Errors in frequency measurement because of counter errors should be much less than 0.1 Hz, which, for a beat frequency of about 2 KHz, is less than ±0.005%. There may have been a difference in the temperatures of the QCMs as high as ±1 K because of uncertainties in knowledge of the respective PRT and silicon diode calibration curves, but a 1 K temperature difference near 85 K would cause only a fractional change in an already negligible evaporation rate of about 10^{-22} g/cm^{2}s (Ref. 11). The condensation coefficient for the two QCMs should be identical, since in both cases material from the same source is impinging on its own condensed phase.

View factor uncertainty can be associated with apparatus nonsymmetry, inaccurate knowledge of apparatus dimensions,

and nonrepeatability of QCM positioning when removed from and reassembled into the apparatus. Apparatus symmetry was verified during checkout to better than ±0.5% using identical 10-MHz QCMs at 85 K, and water as a molecular source. The QCM dimensions are known to better than ±0.13 mm, and so the locations of their crystals relative to their support struts were known to this accuracy. Because of apparatus complexity, the radial distance from the cell orifice to the QCM crystals was difficult to measure to better than ±0.5 mm, which, for a 15-cm nominal radial distance, corresponds to a view factor error of about ±0.7%. The resulting error in calculated relative view factor should be smaller than this, since the radial distance error would affect the view factor for both QCMs. Angular position errors of the QCMs relative to the apparatus centerline are included in the ±0.5% symmetry error. The total error in the calculated relative view factor of 1.053 should be on the order of about ±1.0%. Since the accuracy of the comparison is directly proportional to the accuracy of the relative view factor, it is concluded that, for both 15-A and 15-B, the measured values of S_{15}/S_{10} agree with the theoretical ratio within this range of experimental uncertainty. This compares to the approximately ±2% agreement between calibrated and theoretical mass sensitivity reported in the literature.[6]

The difference between S_{15}/S_{10} for tests 15-A and 15-B is almost certainly because of a difference between actual and calculated view factors from differences in the actual positions of the QCMs after assembly into the apparatus. The two 15-MHz QCMs are geometrically identical, but variations in position relative to the support struts could have occurred between successive assemblies because of excessive bolt hole clearances at the attachment interfaces. A 0.7% difference in view factor would correspond to a quite-probable repositioning variation of 0.5 mm.

References

[1]Garrett, J. W., Glassford, A. P. M., and Steakley, J. M., "ASTM E 1559 Method for Measuring Material Outgassing/Deposition Kinetics," *Journal of the Institute of Environmental Sciences*, Vol. 38, No. 1, 1995, pp. 19–28.

[2]Bargeron, C. B., Phillips, T. E., and Benson, R. C., "Thermogravimetric Analysis of Selected Condensed Materials on a Quartz Crystal Microbalance," *Optical System Contamination: Effects, Measurements, Control IV*, Vol. 2261, Society of Photo-Optical Instrumentation Engineers, July 1994, pp. 188–199.

[3]Glassford, A. P. M., "Practical Model for Molecular Contaminant Deposition Kinetics," *Journal of Thermophysics and Heat Transfer*, Vol. 6, No. 4, 1992, pp. 656–664.

[4]Dyer, J. S., Mikesell, R., Perry, R., and Mikesell, T., "Contamination Measurements During Development and Testing of the SPIRIT III Cryogenic Infrared Telescope," *Optical System Contamination: Effects, Measurements, Control IV*, Vol. 2261, Society of Photo-Optical Instrumentation Engineers, July 1994, pp. 239–253.

[5]Hall, D. F., "Flight Measurement of Molecular Contaminant Deposition," *Optical System Contamination: Effects, Measurements, Control IV*, Vol. 2261, Society of Photo-Optical Instrumentation Engineers, July 1994, pp. 58–71.

[6]Lu, C., "Theory and Practice of the Quartz Crystal Microbalance," *Applications of Piezoelectric Quartz Crystal Microbalances*, Elsevier, New York, 1984, pp. 19–61.

[7]Muller, R. M., and White, W., "Direct Gravimetric Calibration of a Quartz Crystal Microbalance," *Review of Scientific Instruments*, Vol. 39, No. 3, 1968, pp. 291–295.

[8]Muller, R. M., and White, W., "Areal Densities of Stress-Producing Films Measured by Quartz Crystal Microbalance," *Review of Scientific Instruments*, Vol. 40, No. 12, 1969, pp. 1646, 1647.

[9]Glassford, A. P. M., "An Analysis of the Accuracy of a Commercial Quartz Crystal Microbalance," *Thermophysics of Spacecraft and Outer Planetary Entry Probes*, Vol. 56, Progress in Astronautics and Aeronautics, AIAA, New York, 1977, pp. 175–196.

[10]Hirth, J. R., and Pound, G. M., "Coefficients of Evaporation and Condensation," *Journal of Physical Chemistry*, Vol. 64, May 1960, pp. 619–626.

[11]Honig, R. E., and Hook, H. O., "Vapor Pressure Data for Some Common Gases," *RCA Review*, Vol. 21, Sept. 1960, pp. 360–368.

Analytical Expression for a Concentric-Cylinder Radiation View Factor

R. Srinivasan* and Angela C. White†
Air Products and Chemicals, Inc., Allentown, Pennsylvania 18195-1501

Nomenclature

A_i = area of cylinder i
L = distance between the bases of (finite length) rings
r_i = radius of cylinder i
S = length of the ray between a point on one ring and a point on the other ring
z_i = axial coordinate in ring i
z = distance between (differential) rings
α = $(z^2/2r_1r_2) + \frac{1}{2}(\phi_1 + \phi_2)$
β_i = angle between surface-normal of ring i and the ray S that connects the rings
δ_i = length of ring i
θ = azimuthal angle, on the plane of the shell ring
ϕ_1 = r_1/r_2
ϕ_2 = $1/\phi_1$
φ = azimuthal angle, on the plane of the tube ring

Subscripts
1 = tube, i.e., the inner cylinder
2 = shell, i.e., the outer cylinder

Introduction

RADIATION is a major mode of heat transfer in high-temperature processes; the radiation view factor (also known as configuration factor, shape factor, angle factor, etc.) is a key element of the underlying heat balances. Software packages exist (e.g., FACET, VIEW) to find radiation view factors numerically for any complicated configuration, taking obstructions into account.[1] Nevertheless, simple and accurate analytical expressions for the view factor are always of interest. The shell and tube geometry is common to rockets, reactors, heat exchangers, and tubular furnaces. Hence, it can be expected that view factors for this geometry can be found in the literature. Indeed, a literature search revealed several sources.[2–7]

The comprehensive report by Leuenberger and Person[2] includes an expression for the differential view factor between a ring on the tube exterior and the finite annular space on the end plug between the tube and the shell, but none for the differential view factor between a differential ring on the tube exterior and a differential ring on the shell interior. Finding or deriving the latter became the objective of this work.

The expressions derived by Rea[3] or Shukla and Ghosh[4] are for finite view factors between two coaxial cylinders of different lengths that are displaced from one another; the expressions compiled/derived by Brockmann[5] are also for finite view factors between two concentric cylinders of equal lengths. These view factors, which apply to finite cylinders that are end-capped, not to differential ring elements on two concentric

Received June 23, 1995; revision received Sept. 21, 1995; accepted for publication Oct. 30, 1995.

*Research Associate, Air Separation Technology Center, 7201 Hamilton Blvd.

†Currently Graduate Student, Department of Chemical Engineering, University of Texas, Austin, TX 78712.